Desalination and Water Treatment
www.deswater.com
doi: 10.5004/dwt.2020.25846

194 (2020) 187–193
August

Adsorption of selenium (Se^{4+}) ions pollution by pure rutile titanium dioxide nanosheets electrochemically synthesized

Ahmed Mahdi Rheima[a], Mahdi A. Mohammed[b,*], Shaimaa Hamed Jaber[c], Shahad Abbas Hameed[a]

[a]*Department of Chemistry, College of Science, Wasit University, Alkut, Iraq, emails: arahema@uowasit.edu.iq (A.M. Rheima), shad.sa190@gmail.com (S.A. Hameed)*
[b]*Department of Physics, College of Science, Wasit University, AlKut, Iraq, email: mahmed@uowasit.edu.iq (M.A. Mohammed)*
[c]*Department of Chemistry, College of Science, University of Mustansiriyah, Baghdad, Iraq, email: shaemaahamed800@uomustansiriyah.edu.iq (S.H. Jaber)*

Received 18 October 2019; Accepted 17 March 2020

ABSTRACT

In this work, pure rutile titanium dioxide (TiO_2) nanosheets are synthesized by the electrochemical deposition method using a rectangular titanium plate (4 cm × 2 cm × 0.1 cm) as both cathode and anode with a current density of 9.2×10^{-3} mA/cm^2 for 3 h. The rutile TiO_2 nanosheets are investigated by both scanning electron microscopy and transmission electron microscopy measurements, and their crystal structure is obtained using the X-ray diffraction technique. The Brunauer–Emmett–Teller analysis was shown the surface area of the rutile phase was 52 m^2/g. The electrochemical synthesized rutile TiO_2 nanosheets behave as an attractive adsorbent for Se^{4+} ions from their aqueous solutions. We examined the impact of contact time, pH, adsorbent mass, temperature and initial concentration of Se^{4+} ions. The Se^{4+} ions isotherm adsorption showed a good fit with Freundlich isotherm and Langmuir models. The thermodynamic study was done to calculate the ΔS, ΔH and ΔG parameters, which obtained 7.39 kJ/mol, 39.32 J/mol K, and –4.32 kJ/mol, respectively. Moreover, the kinetic study showed the adsorption behaved as pseudo-second-order.

Keywords: Titanium dioxide; TiO_2; Rutile phase; Adsorption; Selenium; Electrochemical method

1. Introduction

Currently, titanium dioxide (TiO_2) is an interesting material, as it has outstanding optical, electrical, photocatalytic and thermal characteristics, especially as adsorbent, catalytic, supercapacitors, lithium-ion batteries and gas sensor [1–7]. The color of pure TiO_2 is close to being white. However, it shows in other colors such as yellow, brown, etc. due to the existence of other metals [8].

TiO_2 crystals can generally be described as three primary phases: anatase (tetragonal), rutile (tetragonal) or brookite (orthorhombic) [9,10]. The distinct physical characteristics of each polymorph are diverse. The rutile phase is the most stable stage under environmental conditions among the three polymorphs, while anatase and brookite can be metastatic at all temperature degrees and become rutile with increasing temperature. Several studies have been shown that different TiO_2 phases are stable that depend on the scale size of their particles. When the nanoparticles are lower than 11 nm, anatase is thermodynamically stable. Nevertheless, rutile and brookite nanoparticles have stable phases at a size of 35 and 11–35 nm, respectively [8,11].

TiO_2 material is stable, noncorrosive, eco-friendly, abundant and cost-effective. It shows to be more promising and most widely used [12–14]. It has been categorized as non-hazardous that has no major adverse health impacts

* Corresponding author.

[15]. Therefore, many researchers have used TiO_2 as the removal of heavy metals from aqueous solutions [16–22]. Selenium is a metalloid element, which intermediates to metals and non-metals [23], and it is a major health micronutrient, but selenium toxicity is a problem at high concentrations [24]. Due to its participation in several industries, selenium is increasingly being removed from the water. The high capability, easy and fast adsorption was shown with nanomaterials. The first study of the selenium adsorption from aqueous solution using nano-TiO_2 material was done by Zhang et al. [21] that showed high adsorption capacity to remove selenium at a percentage of 96% in the pH between 2 and 6.

According to our knowledge, no methodical data on the adsorption behavior of Se^{4+} have been studied using the rutile TiO_2 nanosheets. Due to their interesting dimensions of the rutile TiO_2 nanosheets that were synthesized by the electrochemical method, they were used to separate Se^{4+} from their aqueous solutions. The mass of adsorbent, the period of surface touch, pH, temperature and initial concentration of Se^{4+} ions were considered in this study.

2. Experimental setup

2.1. Materials

Titanium plate, NaOH, HCl, $SeCl_4$ and ethanol were purchased and used as received from Sigma-Aldrich (UK). The deionized water was used throughout the purification of the final product.

2.2. Synthesis of rutile TiO_2 nanosheets

Pure rutile TiO_2 nanosheets were synthesized by the electrolysis using 120 mL of 0.1 M NaOH at 20°C as the electrolyte. A rectangular titanium plate (4 cm × 2 cm × 0.1 cm) was used as an anode and the same dimensions of rectangular titanium plate were used as a cathode. Before mounting the substrates in the cell, they were cleaned by a bath sonication with using aqueous and organic cleaner solvent (ethanol and deionized water) sequentially and each cleaning step duration was 10 min. The applied D.C. voltage between the electrodes was set to be 3 V under a current density of 9.2×10^{-3} mA/cm^2 for 3 h. A white precipitate was obtained and the yielding material was purified using deionized water and then it was dried for overnight to subsequent analysis.

The electro deposition reaction pathway suggestion to form TiO_2 was:

$$Ti \rightarrow Ti^{+4} + 4e^- \quad \text{(at anode)} \tag{1}$$

$$Ti^{+4} + 4e^- \rightarrow Ti^* \quad \text{(at cathode)} \tag{2}$$

Here (Ti*) is an active form of (Ti).

$$Ti^{+4} + 4OH^- \rightarrow Ti(OH)_4 \tag{3}$$

$$Ti(OH)_4 \xrightarrow{Ti^*} TiO_2\,(\text{nanosheets}) + 2H_2O\ (\text{all of them at pH} = 12) \tag{4}$$

2.3. Characterization

The rutile TiO_2 nanosheets were characterized by X-ray diffraction (XRD-6000) that was operated at 30 mA and 40 kV to generate radiation at a wavelength of 1.5406 Å. JEOL JEM-2100 (Japan) transmission electron microscopy (TEM) measurement was utilized to study the morphology of nanosheets. JEOL JEM-6510 LV scanning electron microscopy (SEM) was used to determine the dimensions of TiO_2 flakes. Shimadzu 4800S (USA) Fourier-transform infrared spectroscopy (FTIR) spectrophotometer was shown the spectrum of TiO_2 nanosheets. The surface area of nanosheets was measured using Micromeritics' Gemini VII 2390 (USA) Series of surface area analyzers.

2.4. Adsorption of selenium on rutile TiO_2 nanosheets

Thirty-milliliter solutions were prepared from the stock solution (500 ppm) of Se^{4+} ions at different concentrations between 60 and 110 ppm by dissolving $SeCl_4$ in deionized water. 0.01 g of TiO_2 nanosheets were added to these solutions and shackled for about 40 min at selected temperatures 15°C, 25°C, 35°C, 45°C, and 55°C. These solutions were filtered and used in an atomic absorption spectrometer to identify the concentration of Se^{4+} ions in the filtrate and applied the following equation [22,25]:

$$Q_e = \frac{(C_0 - C_e)V_{\text{sol}}}{M} \tag{5}$$

where Q_e (mg/g) is the equilibrium capacity of adsorption, C_0 and C_e are Se^{4+} ions concentrations (mg/L) initially and at equilibrium, V_{sol} is the volume of liquid (L) and M is the mass of the TiO_2 nanosheets (g).

3. Results and discussion

3.1. Characterization of TiO_2 nanosheets

All samples were subject to XRD to diagnosis the nature of produced powders. The XRD peaks at angles from 20° to 80° of the TiO_2 crystal-style structure is shown in Fig. 1. According to the standard patterns of rutile TiO_2, the high peaks at 27.46°, 36.09°, and 54.34° which are corresponding to 110, 101, and 211 Müller values, respectively. The crystallite dimensions were determined using the Scherrer formula [26,27].

$$S = \frac{k\lambda}{\beta\cos\theta} \tag{6}$$

where k = 0.9 which is Scherrer constant, λ is the wavelength of the Cu-Kα radiation, β corresponds to line broadening in radians (the full width at half maximum) and θ is Bragg angle. The crystal size was calculated to be about 24.6 nm.

The FTIR spectrum of TiO_2 nanosheets is shown in Fig. 2. The band at 500–600 cm^{-1} belongs to the bending vibration (Ti–O–Ti) bonds in the TiO_2 lattice [28]. The peak at 1,653 cm^{-1} relating to bending modes of water Ti–OH. The broadest band, which is observed at 3,373–3,500 cm^{-1},

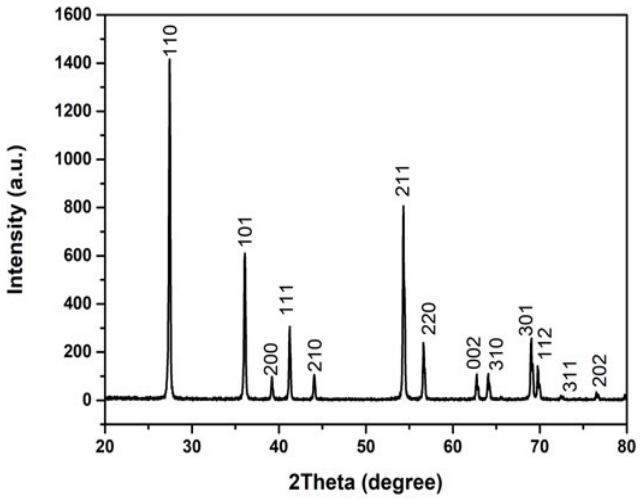

Fig. 1. XRD graph of the rutile TiO_2 nanosheets.

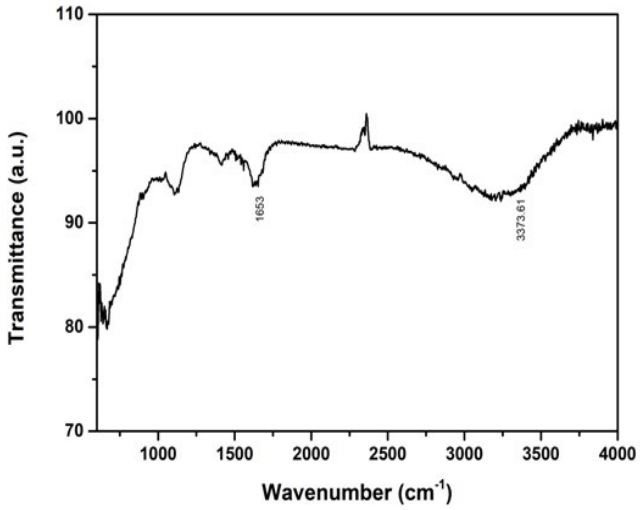

Fig. 2. FTIR spectrum of TiO_2 nanosheets.

corresponds to the stretching vibration of the hydroxyl group O–H on the surface TiO_2 nanosheets [29].

The form and size of the primary nanosheets were assessed by SEM as shown in Fig. 3. The assessment demonstrates that the nanosheets were crystallized well, and they were shown to have clear two dimensions. They show to be close to the rectangular shape with nanoscale thickness. Besides the structure of nanosheets, the figures also show a few amounts of TiO_2 as the shape of nanoparticles. Their average size was determined at about 13 nm. In addition, TEM analysis was carried out on synthesized powders. Fig. 4 shows that aggregation occurs during the process of nanosheet formation. The flakes are shown to have a small thickness at the nanoscale. The Brunauer–Emmett–Teller specific surface area of the rutile phase was found to be 52 m^2/g. This proof is that the specific surface area had a good agreement with a reference TiO_2 nanomaterial p25 (50 m^2/g). The high surface area of the nanosheets gives attention to study their adsorption behavior.

3.2. Adsorption isotherms

The most significant step in the adsorption study was to fit isotherm adsorption with adsorption results to define how adsorbent and Se^{4+} ions interact. In this work, Freundlich and Langmuir's isotherms were considered. The correlation factor R^2 shows that both Freundlich and Langmuir isotherm equations fit very close to the adsorption results as shown in Fig. 5. The linearized form of the Freundlich adsorption was expressed in the following equation [30,31]:

$$\log\left(Q_e\right)=\log\left(k_f\right)+\left(\frac{1}{n}\right)\log\left(C_e\right) \tag{7}$$

where k_f and n, which are called the Freundlich constants, are the indicators of adsorption capacity and adsorption intensity, respectively. The k_f is gotten from the intercept and the n is obtained from the slope.

In this project, the Freundlich isotherm for TiO_2 was calculated $1/n$ which was 0.358. This result agreed with demonstrating favorable physical adsorption [32].

As shown in the below equation, the data were also fitted with the Langmuir adsorption isotherm [33]:

$$\frac{C_e}{Q_e}=\frac{1}{q_{\max}}K_L+\frac{C_e}{q_{\max}} \tag{8}$$

where K_L (mg/L) represents the Langmuir constant regarding the adsorption energy, $q_{\max}$ (mg/g) is the highest amount of Se^{4+} ions adsorbed per gram of adsorbent.

The dimensionless constant (R_L), which is also called the separating factor, exhibits vital characteristics of the Langmuir isotherm and is described as:

$$R_L=\frac{1}{\left(1+K_LC_i\right)} \tag{9}$$

where C_i (mg/L) is the initial concentration of Se^{4+} ions, the R_L values are all within (0–1) that indicate the adsorption of Se^{4+} ions on the TiO_2 nanosheets is preferable.

3.3. Effect of contact time

To achieve a balanced time, the time of contact was determined by mixing 0.01 g of TiO_2 nanosheets with 30 mL of Se^{4+} ions (80 ppm) in a sequence of tests. The mixture was shaken at 200 rpm under 298 K temperature. Fig. 6 shows the adsorption was extremely rapid at the beginning of 10–20 min. The fast adsorption came from a strong link between active TiO_2 and Se^{4+} ions. Because of the occupancy on the TiO_2 surface nanosheets, the adsorption rate of Se^{4+} ions became constant after 40 min.

3.4. Effect of pH

The pH of the Se^{4+} ion solution was a fundamental of the adsorption procedure. In this work, the adsorption impact of pH was determined between 2 and 12. The collected data were plotted as the capacity of adsorption vs. pH as seen in Fig. 7. The graph shows that Se^{4+} ion adsorption in acidic

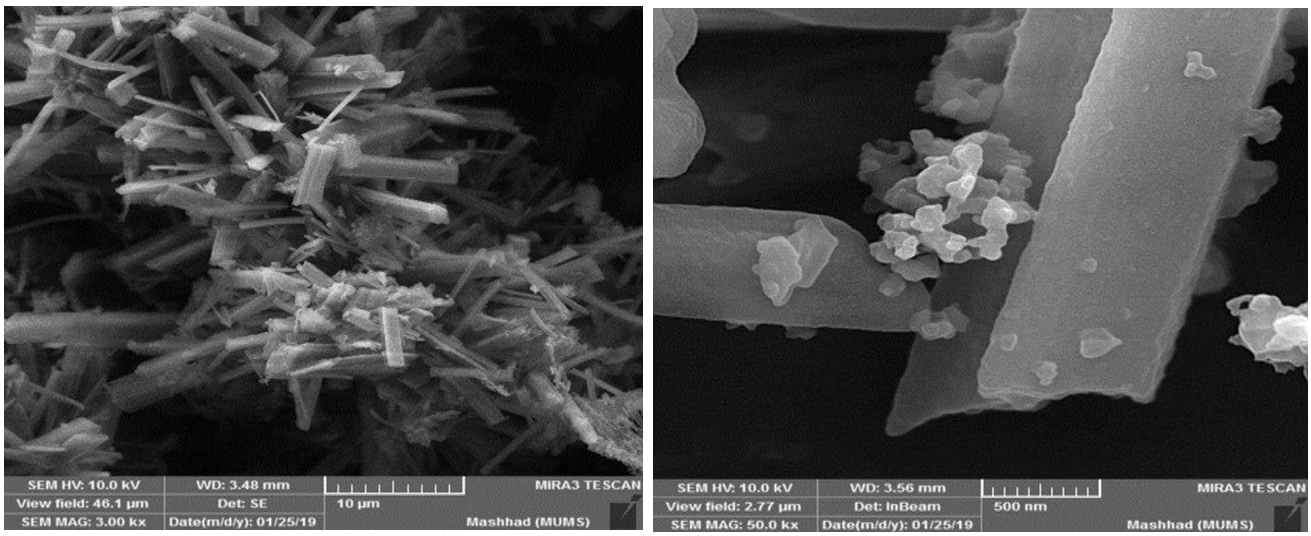

Fig. 3. SEM micrographs of the rutile TiO_2 nanosheets.

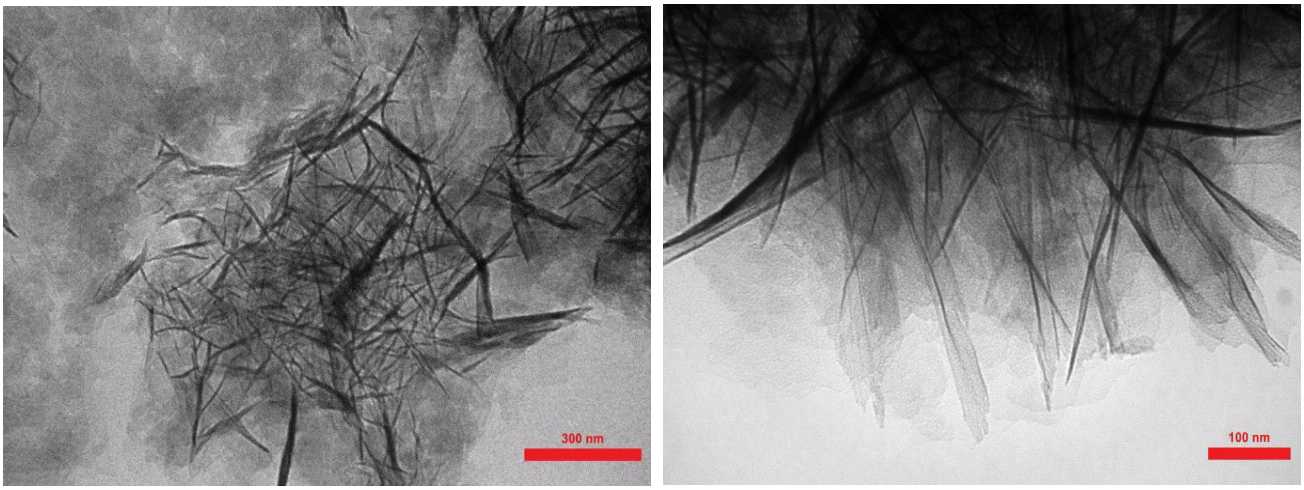

Fig. 4. TEM micrographs of the rutile TiO_2 nanosheets.

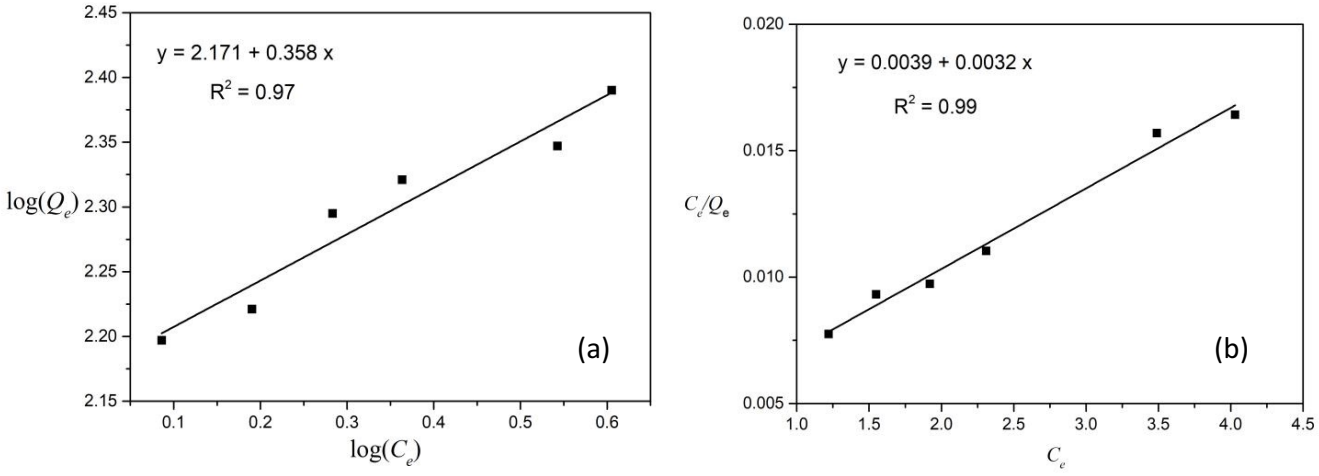

Fig. 5. Adsorption curves of (a) Freundlich isotherm and (b) Langmuir isotherm at 298 K.

mediums was extremely absorbed. At isoelectric point (IEP) [34], the charge on the TiO_2 surface nanosheets was neutral with a pH_{IEP} value of 6.8 for TiO_2 nanosheets. Sorbent surface had a pH value lower than IEP with positive charges. This improves an electrostatic attraction with Se^{4+} ions. The repulsion of negative charge in the sorbent was observed at the highest pH_{IEP} that was a result of the release of adsorbed selenium by TiO_2 nanosheets. The maximum adsorption of selenium was shown at pH range from 2 to 6, and the selection of pH value at 5.5 was carried out for Se^{4+} ions in the experiment.

3.5. Effect of adsorbent mass

The adsorbent mass influence was determined after adding different amounts of titanium nanosheets starting from 0.01 to 0.06 g to 300 ppm of Se^{4+} ions. The mixture was shaken at 200 rpm under 298 K temperature. The amount of adsorbed as a function of mass is shown in Fig. 8. At first, the adsorption rate is rapid owing to the increased amount of active site of TiO_2 nanosheets. Increased adsorption of Se^{4+} ions was shown by increasing the amount of adsorbent mass.

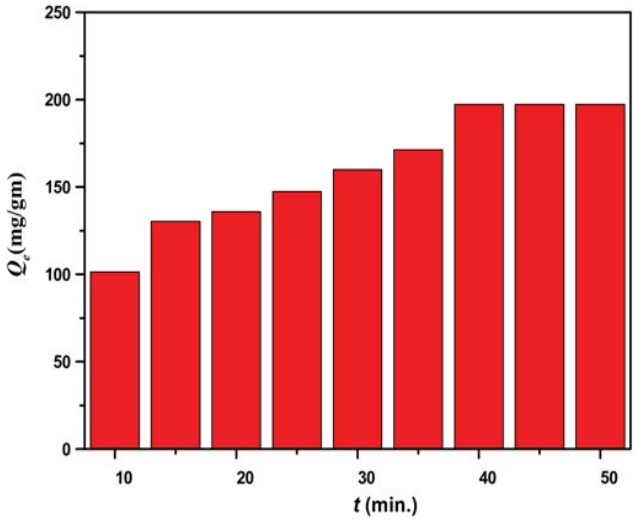

Fig. 6. Effect of time on adsorption of Se^{4+} ions onto TiO_2 nanosheets.

3.6. Temperature effect and thermodynamic parameter calculation

The temperature influence of selenium adsorption on the surface of TiO_2 nanosheets was studied at selected temperatures 15°C, 25°C, 35°C, 45°C, and 55°C. The amount of adsorption solution of Se^{4+} ions increased with increasing temperature. This means the process was endothermic, and the mean of ΔH was positive. This was proof of both absorption and adsorption processes. When the temperature increased, diffusion molecules were absorbed into the pores and rose diffusion rates as well as the strong bond that connects between the adsorbate and the adsorbent [35].

The thermodynamic parameters provide detailed data about the intrinsic energy modifications connected with adsorption and should, therefore, be correctly assessed. In this research, the following variations were calculated to forecast the process of adsorption using the free energy of the adsorption ($\Delta G°$), enthalpy ($\Delta H°$) and entropy ($\Delta S°$), depending on the following equations:

$$\ln\left(K_e\right) = \frac{-\Delta H}{RT} + \frac{\Delta S}{R} \tag{10}$$

$$K_e = \frac{Q_e}{C_e} \tag{11}$$

$$\Delta G = \Delta H - T\Delta S \tag{12}$$

where K_e is an equilibrium constant, R is a gas constant (8.314 J/mol K) and T is the temperature (K). From the slope

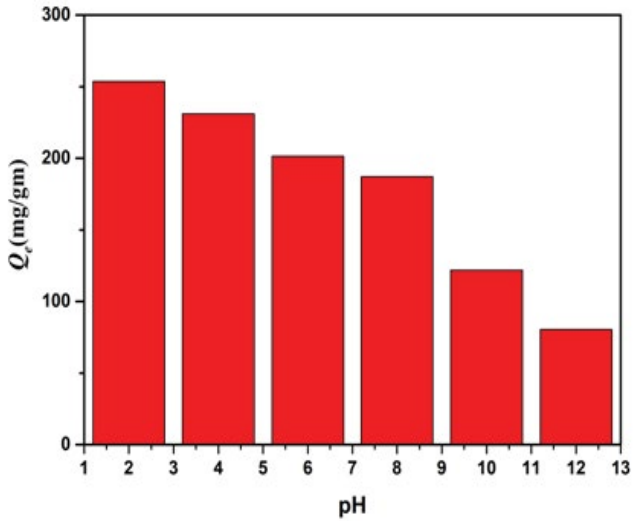

Fig. 7. Effect of pH on adsorption of Se^{4+} ions onto TiO_2 nanosheets.

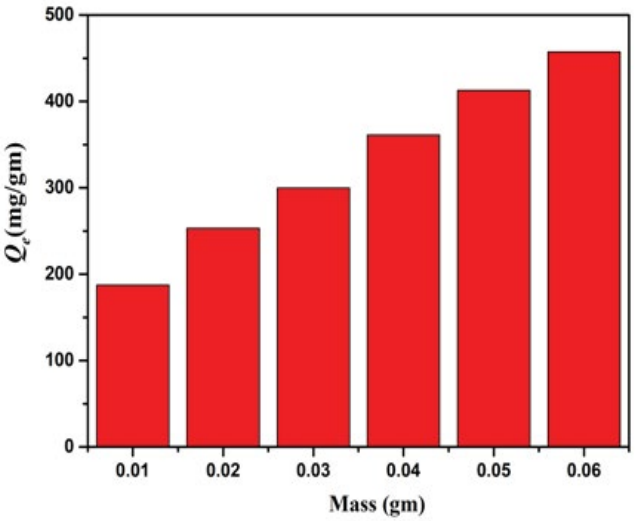

Fig. 8. Effect of adsorbent mass on adsorption of Se^{4+} ions onto TiO_2 nanosheets.

and interception of the plots of van't Hoff, ΔH and ΔS were identified [36] as shown in Fig. 9.

The corresponding ΔH from the slope was 7.39 kJ/mol, which indicated the process was endothermic. The ΔS from the intercept was 39.32 J/(mol K) that indicated the adsorbed molecules were still in constant motion on the surface, and they were attributable to absorption as well as adsorption. A higher temperature facilitated the adsorption of Se^{4+} ions. The ΔG for adsorbing was determined to be –4.32 kJ/mol at 298 K, which means spontaneous adsorption.

3.7. Dynamics

The adsorption dynamics of Se^{4+} ions on the surface adsorbents of TiO_2 nanosheets are crucial in the adsorbent applications. In the study of Se^{4+} ions was found the adsorption equilibrium time was around 40 min for 0.01 g of TiO_2 nanosheets adsorbents.

Furthermore, classical and kinetic models in this study were used to portray the information of adsorption mentioned above as follows:

Pseudo-first-order model [37]:

$$\ln(q_e - q_t) = \ln(q_e) - k_1 t \tag{13}$$

Pseudo-second-order model [38]:

$$\frac{1}{q_t} = \frac{1}{k_2 q_e} + \frac{t}{q_e} \tag{14}$$

where q_e and q_t represent the number of adsorbent Se^{4+} ions (mg/g) at equilibrium and time, respectively, and the k_1 and k_2 values are the kinetic rate constants. The pseudo-second-order model with an elevated correlation coefficient ($R^2 > 0.9622$) can correctly describe the kinetic information, Fig. 10.

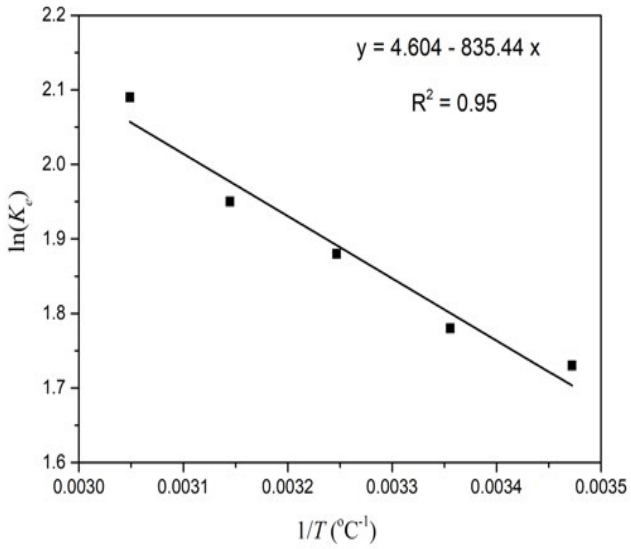

Fig. 9. Relation between $\ln(K_e)$ and $1/T$ for the adsorption of Se^{4+} ions.

4. Conclusion

The electrochemical method showed to produce high quality of the rutile TiO_2 nanosheets according to the XRD, SEM, and TEM characterizations. All the characterization techniques gave identical results to prove that the synthesized nano-TiO_2 was rutile sheets and their average crystal size was calculated to be 24.6 nm. The nanosheets proved to have excellent adsorption properties for removing Se^{4+} from aqueous solutions. Both kinetic and dynamic studies were shown the efficiency of the rutile TiO_2 nanosheets adsorption. The results were fitted well with Freundlich and Langmuir isotherm models. The calculations of the thermodynamic parameters gave the adsorption values for ΔH, ΔS, and ΔG equal to 7.39 kJ/mol, 39.32 J/mol K, and –4.32 kJ/mol, respectively. These results prove that the adsorption is an endothermic spontaneous process and it behaves as pseudo-second-order with $R^2 = 0.9622$.

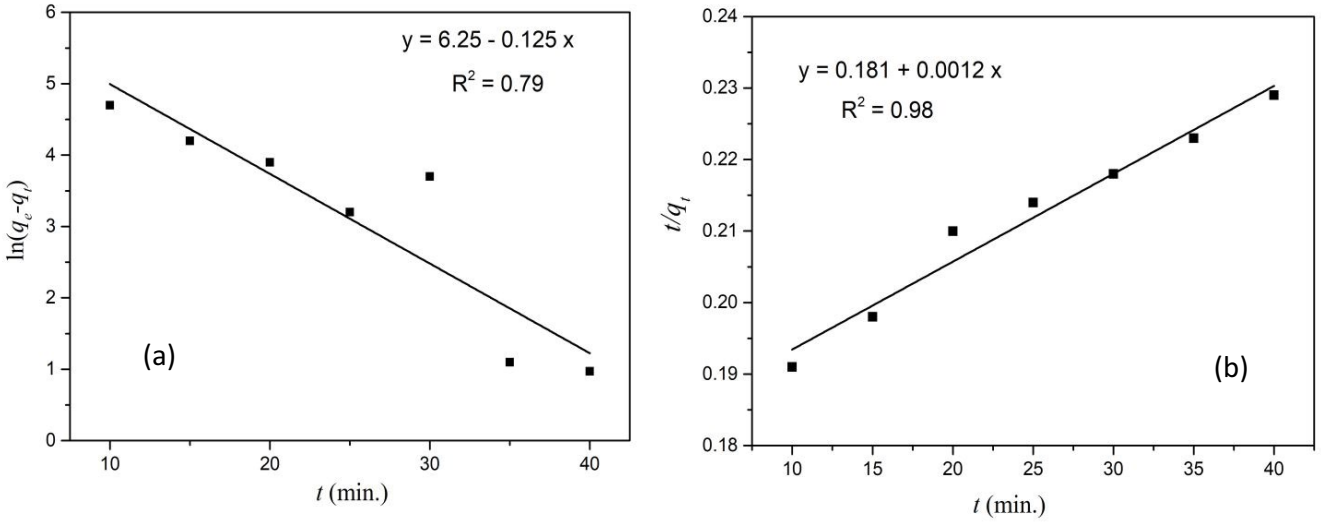

Fig. 10. Dynamic of adsorption of Se^{4+} ions: (a) pseudo-first-order and (b) pseudo-second-order.

References

[1] X.H. Lu, G.M. Wang, T. Zhai, M.H. Yu, J.Y. Gan, Y.X. Tong, Y. Li, Hydrogenated TiO_2 nanotube arrays for supercapacitors, Nano Lett., 12 (2012) 1690–1696.

[2] J.H. Kim, D. Bhattacharjya, J.-S. Yu, Synthesis of hollow TiO_2@N-doped carbon with enhanced electrochemical capacitance by an *in situ* hydrothermal process using hexamethylenetetramine, J. Mater. Chem. A, 2 (2014) 11472–11479.

[3] X.Y. Shen, M. Chen, X.H. Hong, W.D. Wang, Z.K. Qiao, J. Chen, S.J. Fan, J.X. Yu, C.J. Tang, Synthesis and anodic performance of TiO_2-carbonized PAN electrode for lithium ion batteries, Chem. Phys., 530 (2020) 110639.

[4] S.A.M. Chachuli, M.N. Hamidon, M. Ertugrul, Md.S. Mamat, H. Jaafar, N.H. Shamsudin, TiO_2/B_2O_3 thick film gas sensor for monitoring carbon monoxide at different operating temperatures, J. Phys. Conf. Ser., 1432 (2020) 012040.

[5] I. Heng, C.W. Lai, J.C. Juan, A. Numan, J. Iqbal, E.Y.L. Teo, Low-temperature synthesis of TiO_2 nanocrystals for high performance electrochemical supercapacitors, Ceram. Int., 45 (2019) 4990–5000.

[6] Q. Shen, C.Y. Cao, R.K. Huang, L. Zhu, X. Zhou, Q.H. Zhang, L. Gu, W.G. Song, Single chromium atoms supported on titanium dioxide nanoparticles for synergic catalytic methane conversion under mild conditions, Angew. Chem. Int. Ed., 132 (2020) 1232–1235.

[7] A.M. Aljeboree, A.F. Alkaim, Removal of antibiotic tetracycline (TCs) from aqueous solutions by using titanium dioxide (TiO_2) nanoparticles as an alternative material, J. Phys. Conf. Ser., 1294 (2019) 052059.

[8] L.E. Oi, M.-Y. Choo, H.V. Lee, H.C. Ong, S.B.A. Hamid, J.C. Juan, Recent advances of titanium dioxide (TiO_2) for green organic synthesis, RSC Adv., 6 (2016) 108741–108754.

[9] D. Dambournet, I. Belharouak, K. Amine, Tailored preparation methods of TiO_2 anatase, rutile, brookite: mechanism of formation and electrochemical properties, Chem. Mater., 22 (2009) 1173–1179.

[10] G.S.H. Thien, F.S. Omar, N.I.S.A. Blya, W.S. Chiu, H.N. Lim, R. Yousefi, F.-J. Sheini, N.M. Huang, Improved synthesis of reduced graphene oxide-titanium dioxide composite with highly exposed {001} facets and its photoelectrochemical response, Int. J. Photoenergy, 2014 (2014) 1–9.

[11] H.Z. Zhang, J.F. Banfield, Understanding polymorphic phase transformation behavior during growth of nanocrystalline aggregates: insights from TiO_2, J. Phys. Chem. B, 104 (2000) 3481–3487.

[12] M. Rajca, M. Bodzek, Kinetics of fulvic and humic acids photodegradation in water solutions, Sep. Purif. Technol., 120 (2013) 35–42.

[13] K. Nakata, A. Fujishima, TiO_2 photocatalysis: design and applications, J. Photochem. Photobiol., C, 13 (2012) 169–189.

[14] W.-C. Hung, S.-H. Fu, J.-J. Tseng, H. Chu, T.-H. Ko, Study on photocatalytic degradation of gaseous dichloromethane using pure and iron ion-doped TiO_2 prepared by the sol–gel method, Chemosphere, 66 (2007) 2142–2151.

[15] T. Raguram, K.S. Rajni, Effects of varying the soaking duration of Eosin Blue sensitized TiO_2 photoanodes for dye-sensitized solar cells, Optik, 204 (2020) 164169.

[16] S. Bang, M. Patel, L. Lippincott, X. Meng, Removal of arsenic from groundwater by granular titanium dioxide adsorbent, Chemosphere, 60 (2005) 389–397.

[17] M.E. Pena, G.P. Korfiatis, M. Patel, L. Lippincott, X.G. Meng, Adsorption of As(V) and As(III) by nanocrystalline titanium dioxide, Water Res., 39 (2005) 2327–2337.

[18] D. Nabi, I. Aslam, I.A. Qazi, Evaluation of the adsorption potential of titanium dioxide nanoparticles for arsenic removal, J. Environ. Sci., 21 (2009) 402–408.

[19] P.L.A. Guillaume, A.M. Chelaru, M. Visa, O. Lassiné, "Titanium oxide-clay" as adsorbent and photocatalysts for wastewater treatment, J. Membr. Sci. Technol., 8 (2018) 2.

[20] W.L. Zhang, Y. Wu, J. Wang, J. Liu, H.F. Lu, S.J. Zhai, Q.H. Zhong, S.Y. Liu, W.Y. Zhong, C.L. Huang, X.X. Yu, W.H. Zhang, Y.H. Chen, Adsorption of thallium(I) on rutile nano-titanium dioxide and environmental implications, PeerJ, 7 (2019) e6820.

[21] L. Zhang, N. Liu, L. Yang, Q. Lin, Sorption behavior of nano-TiO_2 for the removal of selenium ions from aqueous solution, J. Hazard. Mater., 170 (2009) 1197–1203.

[22] L. Svecova, M. Dossot, S. Cremel, M.-O. Simonnot, M. Sardin, B. Humbert, C. Den Auwer, L.J. Michot, Sorption of selenium oxyanions on TiO_2 (rutile) studied by batch or column experiments and spectroscopic methods, J. Hazard. Mater., 189 (2011) 764–772.

[23] A.B. Kök, M.D. Mungan, S. Doğanlar, A. Frary, Transcriptomic analysis of selenium accumulation in *Puccinellia distans* (Jacq.) Parl., a boron hyperaccumulator, Chemosphere, 245 (2020) 125665.

[24] M. Rovira, J. Giménez, M. Martínez, X. Martínez-Lladó, J. de Pablo, V. Martí, L. Duro, Sorption of selenium(IV) and selenium(VI) onto natural iron oxides: goethite and hematite, J. Hazard. Mater., 150 (2008) 279–284.

[25] M.A. Mohammed, A.M. Rheima, S.H. Jaber, S.A. Hameed, The removal of zinc ions from their aqueous solutions by Cr_2O_3 nanoparticles synthesized via the UV-irradiation method, Egypt. J. Chem., 63 (2020) 5–6.

[26] A.M. Rheima, M.A. Mohammed, S.H. Jaber, S.A. Hameed, Synthesis of silver nanoparticles using the UV-irradiation technique in an antibacterial application, J. Southwest Jiaotong Univ., 54 (2019), https://doi.org/10.35741/issn.0258-2724.54.5.34.

[27] A.M. Rheima, M.A. Mohammed, S.H. Jaber, M.H. Hasan, Inhibition effect of silver-calcium nanocomposite on alanine transaminase enzyme activity in human serum of Iraqi patients with chronic liver disease, Drug Invention Today, 12 (2019) 2818–2821.

[28] L.S. Chougala, M.S. Yatnatti, R.K. Linganagoudar, R.R. Kamble, J.S. Kadadevarmath, A simple approach on synthesis of TiO_2 nanoparticles and its application in dye sensitized solar cells, J. Nano Electron. Phys., 9 (2017) 1–6.

[29] S.S. Al-Taweel, H.R. Saud, New route for synthesis of pure anatase TiO_2 nanoparticles via ultrasound-assisted sol–gel method, J. Chem. Pharm. Res., 8 (2016) 620–626.

[30] D.H. Hussain, A.M. Rheima, S.H. Jaber, M.M. Kadhim, Cadmium ions pollution treatments in aqueous solution using electrochemically synthesized gamma aluminum oxide nanoparticles with DFT study, Egypt. J. Chem., 63 (2020) 2–3.

[31] A.M. Rheima, D.H. Hussain, M.M.A. Almijbilee, Graphene-silver nanocomposite: synthesis, and adsorption study of cibacron blue dye from their aqueous solution, J. Southwest Jiaotong Univ., 54 (2019), https://doi.org/10.35741/issn.0258-2724.54.6.14.

[32] G. Crini, Kinetic and equilibrium studies on the removal of cationic dyes from aqueous solution by adsorption onto a cyclodextrin polymer, Dyes Pigm., 77 (2008) 415–426.

[33] I. Langmuir, The adsorption of gases on plane surfaces of glass, mica and platinum, J. Am. Chem. Soc., 40 (1918) 1361–1403.

[34] Y. Liu, P. Liang, L. Guo, Nanometer titanium dioxide immobilized on silica gel as sorbent for preconcentration of metal ions prior to their determination by inductively coupled plasma atomic emission spectrometry, Talanta, 68 (2005) 25–30.

[35] S.B. Wang, Y. Boyjoo, A. Choueib, Z.H. Zhu, Removal of dyes from aqueous solution using fly ash and red mud, Water Res., 39 (2005) 129–138.

[36] A. Muhammad, A.U.H.A. Shah, S. Bilal, Comparative study of the adsorption of acid blue 40 on polyaniline, magnetic oxide and their composites: synthesis, characterization and application, Materials, 12 (2019) 2854.

[37] A.M. Farhan, N.M. Salem, A.H. Al-Dujaili, A.M. Awwad, Biosorption studies of Cr(VI) ions from electroplating wastewater by walnut shell powder, Am. J. Environ. Eng., 2 (2012) 188–195.

[38] M. Matouq, N. Jildeh, M. Qtaishat, M. Hindiyeh, M.Q. Al Syouf, The adsorption kinetics and modeling for heavy metals removal from wastewater by *Moringa* pods, J. Environ. Chem. Eng., 3 (2015) 775–784.